
CARS MEASUREMENTS AT HIGH PRESSURE IN A CH₄/O₂ JET FLAME

**F. Grisch¹, L. Vingert², P. Grenard², V. Fabelinsky³,
K. Vereschagin³, and M. Oswald⁴**

¹INSA-Rouen, UMR-CNRS 6614 — CORIA
Saint-Etienne du Rouvray 76801, France

²Onera — The French Aerospace Lab.
Palaiseau 91761, France

³General Physics Institute
Russian Academy of Sciences
Moscow, Russia

⁴German Aerospace Center (DLR)
Institute of Space Propulsion
Lampoldshausen, Germany

The combustion process in a high-pressure gaseous methane/gaseous oxygen rocket model combustor was investigated by means of optical and laser spectroscopic measurements as well as numerical simulations. The combustor was operated at a pressure of 1.0 MPa and at two mixture ratios (O/F = 1 and 2). OH* chemiluminescence imaging was applied for a qualitative analysis of the position and shape of the flame brush. For quantitative results, coherent anti-Stokes Raman spectroscopy (CARS) was applied to measure the spatial temperature distribution inside the combustion chamber. H₂ and H₂O molecules were probed simultaneously using two synchronized broadband CARS setup. Temperatures were derived from the H₂ and H₂O single-shot CARS spectra. Furthermore, the Transported Partially Stirred Reactor (TPaSR) model has been employed for simulations at the same operating conditions. The comparison of the numerical simulations to the experimental temperature distributions shows already qualitative agreement although further improvements are still needed.

1 INTRODUCTION

Progress in liquid rocket propulsion technology during the last century has allowed extensive commercial utilization of space and a continuous growth of the launching market of telecommunications and Earth observation satellites. Developments in space transportation systems have initially relied on full-scale

testing accumulated experience, engineering analysis, and application of basic combustion principles. In this context, research performed during the last twenty years has brought new insights on the processes controlling combustion in high-performance rocket motors. While early research into liquid rocket motors relied heavily on full-scale testing with some model-scale experiments but with limited diagnostic and data acquisition capabilities, recent effort has exploited new model-scale facilities and a set of optical and advanced laser diagnostics. This research has mainly concerned the cryogenic propellant combustion under sub-critical and supercritical conditions, in particular in the case of liquid oxygen (LOx) and gaseous hydrogen (GH₂) injected from a single element at various chamber pressures (0.1–6.0 MPa) [1, 2]. All these experimental studies provided useful information on various processes like the flame structure, ignition, and kinetics inside the combustion chamber. The choice of H₂ as liquid fuel was dictated because of its highest specific impulse compared to other fuels. This advantage, however, is compromised in part by other performance characteristics such as cryogenic and low-density properties, costs, and difficulty of handling. One solution that seems to offer the best development perspectives in the field of aerospace propulsion is the use of hydrocarbons together with LOx in substitution of actual propellants. Hydrocarbons, in fact, are nontoxic, easily storable and handled and possess even higher density and thrust performance than liquid hydrogen or hypergolic propellants. Moreover, their properties are very interesting for the realization of future high-performance Reusable Launch Vehicles (RLV). It is for these reasons that many aerospace agencies and industries in Europe are interested in the development of LOx/HC combustion technologies. Among hydrocarbons, methane is one of the best suitable candidates because of its high specific impulse. Moreover, it represents the simplest hydrocarbon fuel for investigating various physical processes related to rocket combustor technology such as regenerative cooling [3], kinetics of LOx/CH₄ [4], propellant injection [5], and ignition [6].

With respect to these perspectives, an extensive research program was undertaken in order to obtain a better understanding of the methane/air combustion mechanisms at high pressure conditions. This activity was included in the framework of the European program ISP-1 named “In-Space Propulsion” resulting from a scientific research program on combustion in liquid rocket engines [7]. The aim of this project is thus not focus on access to space, but rather deal with propulsion systems required in the subsequent phases of space missions, once the spacecraft or the upper stage has already been placed in orbit.

The present paper reports recent experimental investigations of high-pressure methane/air combustion. The objective of these investigations was to obtain experimental data than can be used to validate model and simulation codes for LOx/CH₄ combustion. In particular, the combustion processes involved in such combustion requires quantitative experimental data measured under well-known conditions. This information can be accessed using noninvasive optical diag-

nostics which offer the capability of temporal and spatial nonintrusive resolved measurements. Among various laser-based diagnostics currently under development for quantitative measurements in flames, CARS spectroscopy is largely used because it is the most accurate and reliable technique providing temperature and major species concentration characterization with high spatial and temporal resolution in complex combustion devices. Examples of successful applications of CARS for temperature measurements in subcritical and supercritical LOx/GH₂ combustion can be found in literature [8–11]. The current paper reports temperature CARS measurements based on the spectra of hydrogen and water vapor in a CH₄/O₂ flame in the Mascotte test facility used for basic investigations of cryogenic combustion in rocket engines [12, 13]. Complementary OH* chemiluminescence measurements were carried out to visualize the flame structure. The experimental data were finally compared to numerical results calculated with simulation models and computer codes capable of treating high-pressure methane/oxygen flames over the entire range of fluid thermodynamics states.

2 EXPERIMENTAL TEST HARDWARE AND PROCEDURE

2.1 Mascotte Combustion Chamber, Version V05

The Mascotte test facility is operated with a single injector head and is dedicated for quantitative and qualitative investigations of sub- and supercritical injection and combustion studies with conventional propellants, usually LOx and GH₂. Its development was achieved progressively, with increasing complexity. Five successive versions were built up, each successive one representing a new step towards operating conditions closer to actual rocket engines. The first three versions allowed the experimental characterization of LOx/GH₂ combustion in sub- and supercritical conditions. Version V04 was modified to study the LOx/CH₄ combustion. The fuel feed line comprising a heat exchanger specifically designed to continuously cool a mass flow rate of 100 g/s of hydrogen from ambient temperature to 100 K during a test duration of 30 s with the third version (V03) has been adapted to liquefy methane at the maximum mass flow rate of 250 g/s, value corresponding to typical specifications of gas generators, (i. e., injection of liquid methane together with LOx). In the last version (V05) currently used in this study, a gaseous oxygen line was further implemented on the test facility to offer perspectives to study gaseous propellants combustion at high pressure.

2.2 The High-Pressure Combustor

The high-pressure combustion chamber was designed and extensively fired at pressures up to 10 MPa. This one consists of an association of a combustion

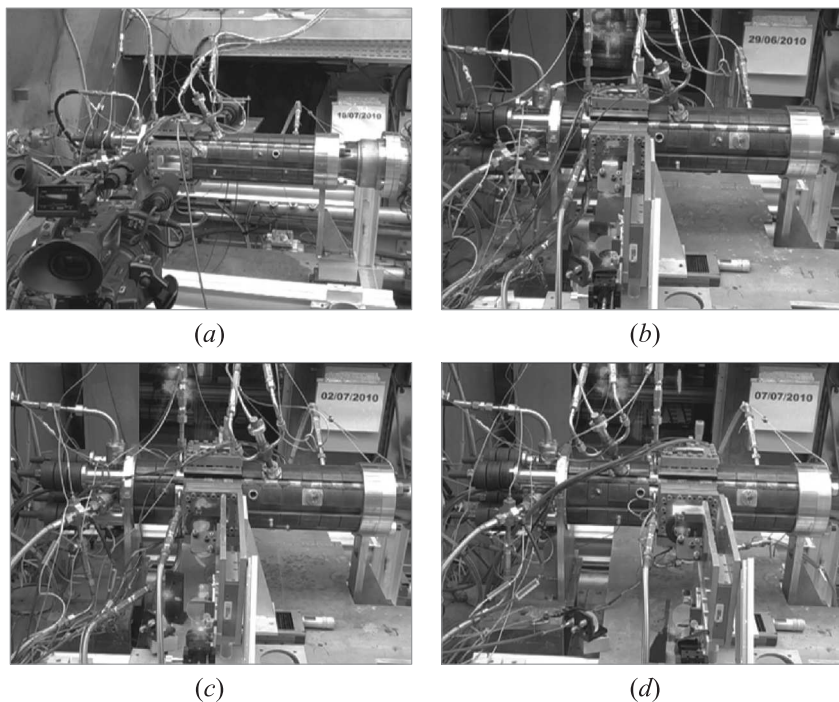


Figure 1 The Mascotte combustion chamber: positions 1 (a); 2 (b); 3 (c); ; and 5 (d)

chamber module with optical accesses enabling the application of nonintrusive optical diagnostic techniques with interchangeable metallic modules. The visualization module is a 50-millimeter square duct, made of stainless steel and fitted with 4 fused silica windows. The two lateral windows are 100 mm long and 50 mm wide. Their internal face is cooled by means of a gaseous N_2 film. The upper and lower windows, for longitudinal laser sheet access, are 100 mm long and 10 mm wide. The visualization module is connected with different interchangeable metallic modules, which enables the optical exploration of the whole flowfield by moving the visualization module at various longitudinal locations. For instance, Fig. 1 displays the combustion combustor and the optics used to send and to focus the laser beams inside the combustion chamber. In the current experiment, temperature measurements were performed for three spatial locations. In position 2, the probe volume is located at 65 mm downstream of the injector exit while positions 3 and 5 correspond to distances of 105 and 210 mm, respectively. Imaging of the flame emission is applied in position 1 for qualitative characterization of the near-injector process. Interchangeable nozzles are

placed at the exit of the combustion chamber and chosen according to the desired pressure level inside the combustion chamber. The nozzle is usually made of graphite, but copper ones are also available. They are either water-cooled or heat sink. The combustion chamber is designed with a simplified thermomechanical model for ensuring sufficiently long duration runs (30 s) at atmospheric pressure, with a maximum mass flow rate of 120 g/s at a mixture ratio of 6. This test duration is reduced to 20 s at higher pressure. The combustor can be fired 6 to 10 times every day, with a time delay of 5–10 min between two successive runs. The combustion chamber is mounted horizontally and its centerline corresponds to the x -axis with the origin representing the exit of the injector. The y - and z -axes are diametrical to the combustor cross section with the y -axis corresponding to the propagation axis of the laser beams inside the combustion chamber. Propellants are ignited with a gaseous H_2/O_2 torch igniter mounted at the top of the combustion chamber.

2.3 Operating Conditions

Figure 2 displays the operating domain of the Mascotte facility (V05) representing the gaseous O_2 /gaseous CH_4 mass flow rates diagram. This diagram shows the available flow rates for both fresh gases, the mixture ratio limits, pressure contours ($P = const$) as well as momentum ratio isocontours ($J = const$). The isobaric lines are calculated for a nozzle throat diameter of 12 mm. The iso- J lines, where J corresponds to the momentum flux ratio $J = \rho V_{CH_4}^2 / (\rho V_{O_2}^2)$, are computed for a standard coaxial injector with the following dimensions: LOx postinner diameter $D_l = 5$ mm, LOx postouter diameter $D_n = 5.6$ mm, CH_4

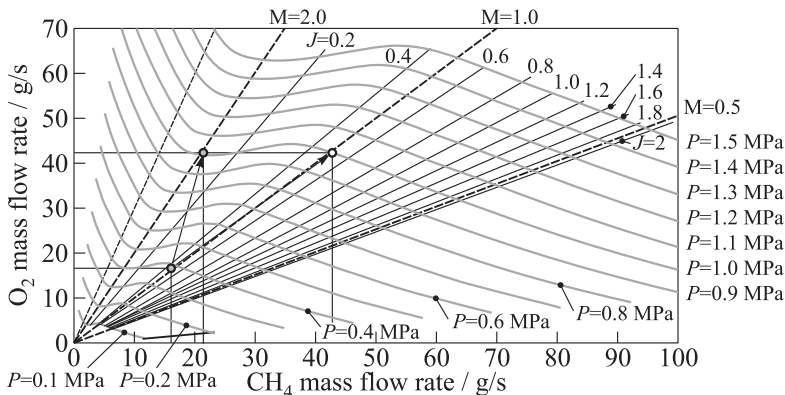


Figure 2 Operating domain of the Mascotte facility (V05) Nozzle throat diameter: $D_c = 12$ mm; injection temperature: $T_{injCH_4} = T_{injO_2} = 288$ K; and injector: $D_l = 5.0$ mm, $D_n = 5.6$ mm, and $D_g = 9.0$ mm

sleeve-outer diameter $D_g = 9$ mm, and both propellants are injected at room temperature, i. e., at 288 K.

The operating mass flow rates of CH_4 and O_2 are chosen for test conditions corresponding to operation at 1.0 MPa. These ones were defined according to two experimental constraints, one consisting in a thermal preservation of the combustion chamber during a hot-fire combustion test and the other one in the optimization of the amount of H_2 and H_2O concentrations for the improvement of temperature CARS measurements. For this purpose, the gaseous species composition in thermodynamics equilibrium conditions for a CH_4/O_2 combustion at 1.0 MPa, and for mixture ratios (O/F) ranging from 0.1 to 10 are computed with the ONERA thermodynamic equilibrium code named Coppelia [14]. Figure 3 shows the behavior of temperature and mass and molar fractions of CH_4 ,

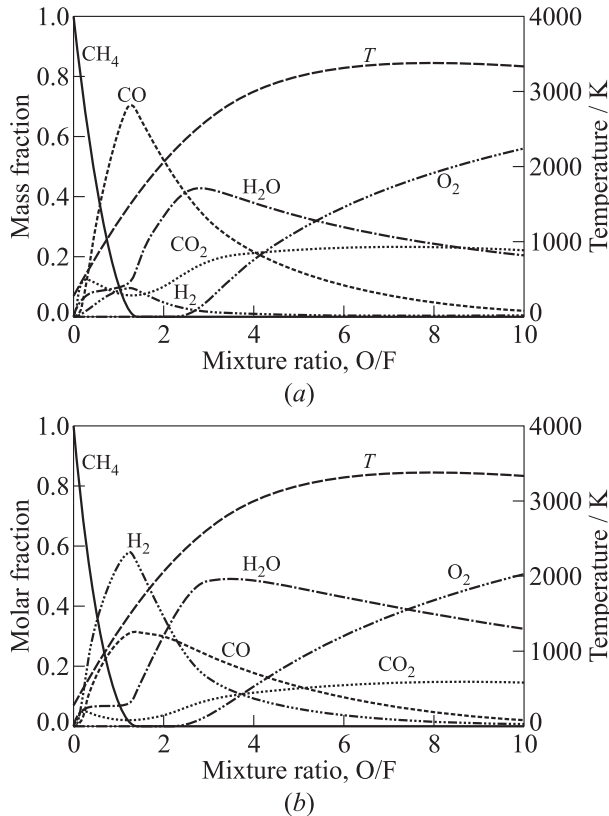


Figure 3 Distribution of temperature, mass and molar fraction of chemical species vs. mixture ratio: 1 — CH_4 ; 2 — O_2 ; 3 — H_2O ; 4 — CO_2 ; 5 — CO ; 6 — H_2 ; and 7 — T

O₂, H₂O, CO₂, CO and H₂ with the mixture ratio. An examination of these behaviors displays a large production of H₂ for a mixture ratio range between 0.5 and 2.5. On the contrary, the production of H₂O appears significantly at O/F = 0.5 and then reaches a maximum for a mixture ratio of 3. Furthermore, the maximal temperature of 3000 K limits hot-fire combustion test for mixture ratios exceeding O/F = 3. An optimization of the permitted values of [H₂] and [H₂O] with temperature allows to identify mixture ratio ranging between 1 and 2 in which measurements are accessible with safety and accuracy.

Test conditions selected for the current experiment at 1.0 MPa are summarized in Table 1. The methane mass flow rate is fixed to 40 g/s for O/F = 1 and 20 g/s for O/F = 2 while the mass flow rates of nitrogen and oxygen are kept constant. The N₂ film mass flow rate needed to thermally isolate the optical windows from the flame front is set to 15 g/s for each mixture ratio. These test conditions slightly differ from the ones simulated and presented in Fig. 1 in which no N₂ film has been taken into account in the simulation. Indeed, the experimental pressure inside the combustion chamber may exceed by 10%–20% the theoretical pressure of 1.0 MPa due to some expected effects of the mixing of N₂ with the reactive products. In case the N₂ stream is diluted via a preferential diffusion process, a full mixing of N₂ with the reactive products will be noted leading then to the heating of the neutral gas and an increase of the total pressure inside the combustion chamber.

Table 1 Definition of operating conditions

Fraction	Mass flow rate, g/s	
	O/F = 1	O/F = 2
O ₂	40	40
CH ₄	40	20
N ₂	15	15

3 EXPERIMENTAL RESULTS

3.1 OH* Radical Chemiluminescence Imaging

Information on the location and structure of the reaction zones in the CH₄/O₂ flame is obtained by recording the flame emission in appropriate emission wavelengths. The chemiluminescence emission of OH* which is emitted in the near ultraviolet (UV) spectral region between 306 and 320 nm [15] and well isolated from the spontaneous emission of oxygen, water, and hydrocarbon molecules is selected to monitor the flame emission during the hot-fire combustion test. OH* chemiluminescence imaging is performed with two detection systems, one image-intensified charge coupled device (ICCD) camera, and one high-speed complementary metal oxide semiconductor (CMOS) camera. The ICCD camera operates with a repetition rate of 4 images per second and allows the record of the OH* chemiluminescence signals with a high dynamic range (16 bit). In opposition, the high-speed CMOS camera permits the visualization of the dynamics of

the flame with a repetition rate of 6000 frames per second but with a reduced dynamic range (12 bit). Both cameras were equipped with an achromatic UV lens (Nikkor UV $f = 105$ mm, $f/4.5$). A UG-5 Schott glass filter blocks radiation above 400 nm and two WG 305 Schott filters complete the suppression of the optical radiation below 283 nm while passing 306 and 320 nm OH* emission bands. Both cameras are installed on both sides of the combustor at right angles with respect to the flow axis.

A selection of instantaneous OH* chemiluminescence images of the reactive mixing layer recorded in position 1 with the ICCD camera is presented in Fig. 4 for both mixture ratios. The exposure time for the image intensifier was set to 1 μ s to capture the instantaneous emission of OH* integrated over the line of sight (i. e., over a line perpendicular to the flow axis). The injector geometry is shown to scale and the complete height of the chamber is displayed. The flow is from left to right with oxygen flow in the center surrounded by coaxial methane stream. Whatever the mixture ratio condition, the OH* emission, and therefore, the reaction zone, starts right on the injector lip and remains very close to the gaseous O₂ jet for some distance. As the flowfield develops downstream, the reaction zone widens slightly. The turbulence of the combusting flow is manifested by the presence of large structures that are readily observable in the instantaneous images. The dimensions of these large-scale structures are of the order of the diameter of the injection nozzle. An analysis of the flame emission in the region nearly close to the injection systems seems to indicate that the flame is attached to the injector lip whatever the mixture ratios. This result is confirmed by complementary dynamic OH* emission measurements performed with the CMOS camera. The high-speed instantaneous OH* emission images shows a reaction zone continuously anchored onto the lip of the injection system, confirming that these flames are stable in the current mixture ratios investigated.

Average and root mean squared (rms) OH* emission spatial distribution over 35 instantaneous OH* images recording during the same hot fire test with the ICCD camera have been obtained. Examples of results shown in Fig. 4 reveal that the flame shape is not really modified by the increase of the mixture ratio from O/F = 1 to 2. The average images recorded in position 1 confirm that OH* chemiluminescence appears in the vicinity of the injection face whatever the mixture ratios. The radial expansion is nearly the same for both mixture ratios. Only the rms values of chemiluminescence intensity reveal a turbulence level higher for O/F = 2 than for O/F = 1. The averaged thickness of the flame can be estimated from the rms OH* emission image which can be attributed to the average temporal displacement of the reactive mixing layer. For instance, an examination of the image displayed in Fig. 4 for O/F = 1 clearly shows a progressive thickening of this reactive zone as the flow develops downstream.

Significant differences between both mixture ratios on the flame structure appear when the optical windows are located in position 5. For O/F = 1, the

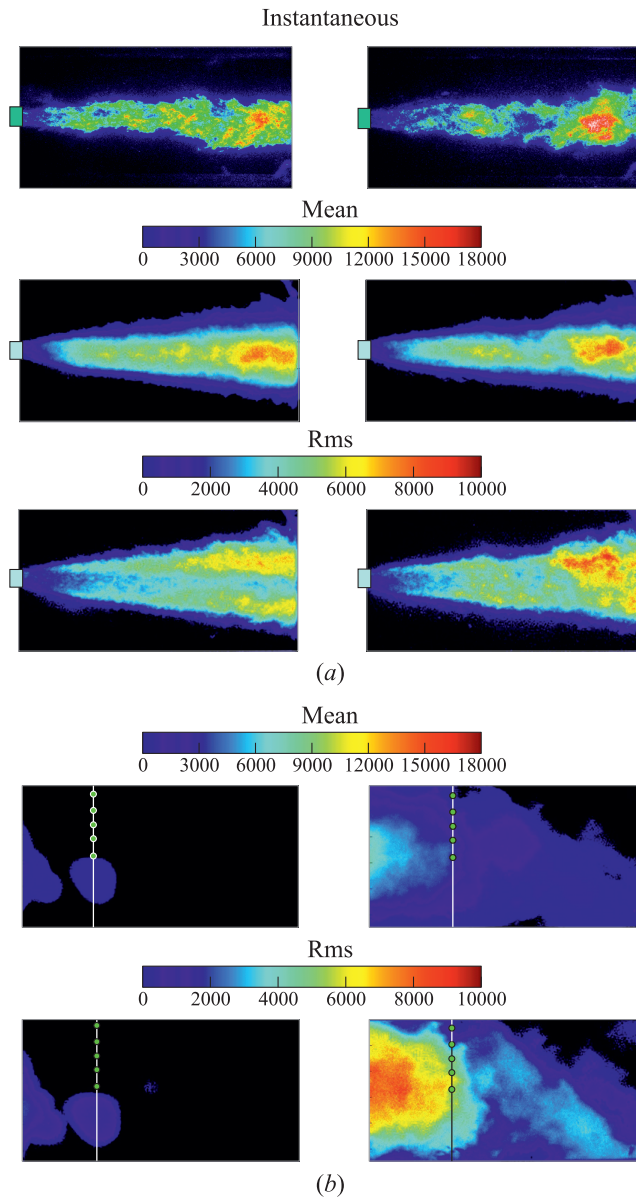


Figure 4 Mean and rms OH* images for mixture ratio $O/F = 1$ (left) and $O/F = 2$ (right). Optical windows positioned in positions 1 (a) and 5 (b).

flame is found to be completely closed, while a large emission of OH* subsists for O/F = 2. However, both average and rms OH* signals show that the flame closure is not far from this region as seen in Fig. 4. The detection of OH* signals in this region is attributed to probable combustion intermittencies induced by a high level of turbulence encountered in these experiments.

3.2 Coherent Anti-Stokes Raman Scattering Thermometry

Coherent anti-Stokes Raman scattering has received considerable attention over the last two decades for combustion diagnosis based upon the pioneering investigations of Regnier and Taran [16]. Excellent review papers and textbooks are available that deal with CARS theory, derive expressions for the signal intensity observed in real experiments, and describe the numerous technical approaches in practical measurements systems [17–20]. The CARS is an example of a four-wave parametric process in which three waves, two at the pump frequency (ω_p) and one at the Stokes frequency (ω_S), are focused to the measurement point in the sample to produce a new coherent beam at the anti-Stokes frequency ($\omega_{aS} = 2\omega_p - \omega_S$). The strength of the interaction depends on the third-order susceptibility of the medium, which is greatly enhanced when the frequency difference ($\omega_p - \omega_S$) matches a Raman active vibrational resonance in the medium. The nonlinear susceptibility is density and temperature-dependent providing the basis of diagnostics. Measurements of medium properties are performed from the shape of the spectral signatures and/or intensity of the CARS radiation. Temperature information derives from spectral shapes and can be extracted from any of the number of molecular constituents. In air-fed combustion, it is most common to perform thermometry from nitrogen since it is the dominant constituent and present everywhere in large concentration despite the extent of chemical reaction. For gaseous oxygen/gaseous methane rocket engine applications, the possible Raman-active probe species are CH₄, H₂, H₂O, and O₂. In case the combustion is operated in fuel-rich conditions (i. e., current experiment), hydrogen is rapidly produced via chemical processes in large concentration in the combustion chamber. O₂ is only present in the core jet while the major product of combustion, H₂O, is available in abundance everywhere. The last candidate, CH₄, is only present in the region located just downstream from the injector. The present authors concentrated their efforts on simultaneous and synchronous CARS of H₂ and H₂O because this gives valuable information on the mixing processes in the turbulent reacting flow.

H₂ and H₂O were already widely used as probed molecules in the past for CARS temperature measurements in sub- and supercritical LOx/GH₂ cryogenic combustors because of their abundance [3, 5, 6]. In the current experiment, the same molecules were probed using a laser system composed of two separate optical benches producing the pump and Stokes beams required for H₂ and H₂O

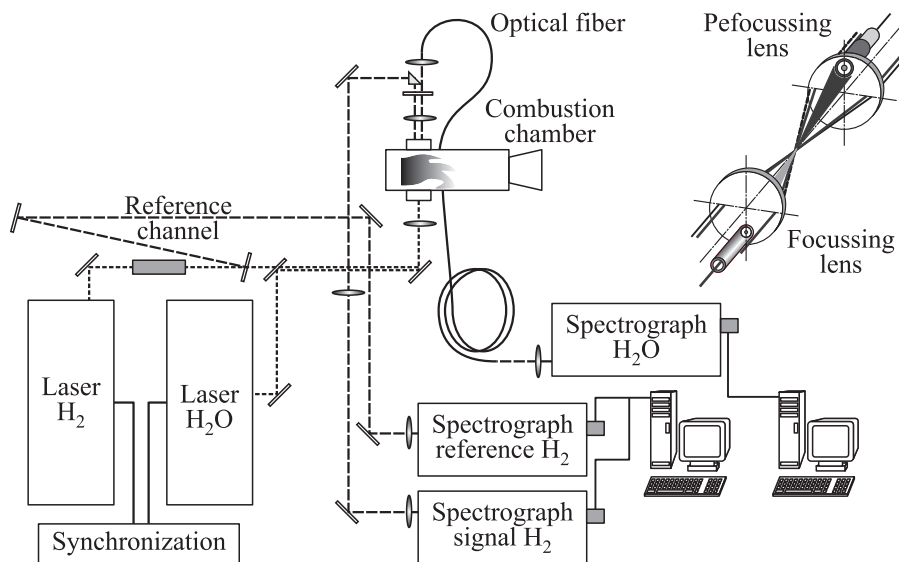


Figure 5 The CARS experimental setup. Jitter ≤ 200 ns; laser beam arrangement: H_2 — planar BOXCARS, H_2O — USED-CARS; and probe volume dimensions: H_2 — $0.8 \text{ mm} \times 100 \mu\text{m}$; H_2O — $2 \text{ mm} \times 150 \mu\text{m}$

CARS spectroscopy (Fig. 5). For H_2 , the pump beam is the doubled-frequency output of a Nd:YAG laser chain composed of a single-mode Q-switched oscillator followed by an amplifier. The laser delivers 140 mJ in 13-nanosecond pulses with a frequency rate of 10 Hz. Half of the green energy is used to pump the Stokes dye. The broadband Stokes beam is centered at 683 nm to excite the Q-branch of hydrogen with a 200 cm^{-1} bandwidth (FWHM, full width at half maximum). At the output of the laser bench, the pump beam is split in two parallel beams and one of them is overlapped with the Stokes beam (planar BOXCARS arrangement). The energy per pulse of the laser beams is typically 30 mJ for each of the pump beams and 4 mJ for the Stokes one. All beams have parallel polarizations. The second laser bench used to probe H_2O consists of a broadband dye laser pumped by a multimode Nd:YAG laser. The pump laser is a Quanta-Ray DCR 3D Nd:YAG unstable oscillator–amplifier system whose multimode output is frequency-doubled to produce a 532 nm laser pulse with a duration of 8 ns. Part of the green laser beam is used to pump a broadband dye laser with mixture of pyridine–methanol and dicyanomethylene (DCM)–methanol dyes providing Stokes radiation with a maximum adjusted near 665–675 nm and a spectral bandwidth of $\sim 580 \text{ cm}^{-1}$. The laser beams are then combined in the USED-CARS (Unstable-resonator Spatially Enhanced Detection) beam geometry: a 15-millimeter diameter, 20 mJ/pulse 532-nanometer donut-shaped pump beam

overlapped coaxially with a 6-millimeter diameter, 10 mJ/pulse Stokes beam. Both laser systems are synchronized at 10 Hz with a time delay of 100 ns and a temporal jitter of 300 ns.

The H₂ laser beams are focused first in air where a nonresonant CARS signal is created to monitor the shot-to-shot fluctuations of direction and of pulse energy of the lasers beams and of the spectral shape of the Stokes laser. Then, the reference signal is split off and the resultant laser beams are combined spatially with the H₂O laser beams. All laser beams pass to the testing facility through optical windows where they are focused in the chamber by means of a single 160-millimeter-focal-length achromat yielding a 0.8-millimeter-long and 50-micron diameter probe volume for H₂ and 2-millimeter-long and 100-micron diameter for H₂O (see Fig. 5). The focal volume is positioned axially and radially in the combustion chamber by moving the optical lenses by means of translational stages. The pump and Stokes beam pulse energies, 12 and 1.6 mJ, respectively, prevent any damages of optical windows and laser-induced breakdown into the flowfield. For H₂O, the pump beam energy is adjusted using a rotating zero order half wave plate and a Glan-Thompson prism while the Stokes beam energy is set fixed. Energies at the probe volume are typically 18 mJ for the pump beam and 4 mJ for the Stokes beam. Reference and sample H₂ CARS spectra are collected and dispersed using two spectrometers equipped with holographic gratings (2100 grooves/cm, radius of curvature 800 mm). The H₂ CARS spectrum and the broadband reference are detected by means of 1340-photodiode arrays. The H₂O CARS signal which is geometrically isolated from the H₂ CARS signal was focused into a single 550-micron diameter quartz fiber by means of a 120-millimeter focal length lens. The fiber guided the CARS signal onto a 1-meter spectrograph equipped with a 1200 grooves/cm grating. The H₂O CARS spectra are recorded using an intensified gated diode array. Both data acquisition systems were started using a single external trigger.

As was mentioned earlier, H₂ and H₂O CARS spectra were simultaneously recorded during each hot fire combustion test. These spectra were used for providing a qualitative picture of the mixing and burning processes in the combustion chamber as well as for temperature measurements. For the latter purpose, the H₂ and H₂O CARS spectra are analyzed with specific spectral processing programs to deduce gaseous temperature. The description of the data processing has been extensively detailed elsewhere [10]. In brief, the H₂ and H₂O CARS spectra in the temperature and pressure range investigated during the experiments are calculated. These calculations use the spectroscopic parameters of each molecule as well as the collisional processes induced by pressure. After creating the database, the calculated spectra are then convoluted with the experimental apparatus function. For the chamber pressure of 1.0 MPa, a library of theoretical spectra was generated at 50-kelvin increments over the range 300–3000 K. For H₂O, libraries were also calculated for various molar fractions of H₂ and H₂O to take into account the effect of the species composition

on collisional linewidths. Temperatures were deduced by fitting the experimental CARS spectra to the theoretical ones using a nonlinear least-squared fitting procedure.

3.3 Coherent Anti-Stokes Raman Scattering Results

The CARS measurements were carried out for both operating conditions and for positions 2, 3, and 5 corresponding to downstream distances $x = 65, 105,$ and 210 mm from the injection exit plane. Five radial distances were investigated for each profile: $y = 0$ (along the flow axis), $5, 9, 13,$ and 16.5 mm. For each molecule, an ensemble of 150 single-shot CARS measurements was recorded during each hot-fire combustion test. The validation rate of the measurements, defined as the ratio between the number of CARS spectra successfully processed and the total number of measurements during one engine test run, ranges between 60% and 100% for H_2 while a validation range larger than 80% is observed for H_2O . These effects were found to be dependent on the probing location within the combustion chamber:

- (i) the validation rate of the H_2 CARS measurements increases along the flow axis; and
- (ii) for each downstream distance, the validation rate of CARS measurements generally increases from the flow axis to the wall.

The expected reasons explaining the variations of the validation rate are the following:

- (i) large variations of production of H_2 and H_2O are present inside the combustion chamber. The amount of these species concentrations display the degree of progress of chemical reactions with the distance downstream from the injector which depends primarily on the mixing of CH_4 and O_2 . The CARS signals are then affected, preferentially for measurements performed at $x = 65$ and 105 mm and for radial positions along and close to the flow axis ($y = 0$ to 9 mm). Above $y = 9$ mm, the validation rate is then maximal. The same goes for distances further away, the validation rate becomes maximal along with the radial displacement of the probe volume from the flow center to the periphery demonstrating the presence of a homogeneous mixture of hot gases at these locations; and
- (ii) beam steering effect can also be observed in the chosen operating conditions. Large density gradients can exist between the oxygen core jet and gaseous methane outer stream. The gradients can cause beam defocusing and also deflection with subsequent loss of signal production. Unsteady

flame and turbulent flow behavior contributes to the beam steering problem, which results in disparities in shot-to-shot measurements. A loss of signal can then be observed, particularly, in positions $x = 65$ and 105 mm where turbulent combustion is intense.

An analysis of the resultant single-shot temperature measurements with time shows no evidence of a temperature evolution during a combustion run indicating that the combustion process is stationary. Similarly, the absence of change in mean temperature recorded for different successive runs on the same operating conditions validate the reproducibility of the combustion process and, thus, permits comparisons between the temperatures measured at various positions. Figure 6 displays examples of histograms of shot-to-shot temperature distributions recorded for five radial positions at a distance of $y = 210$ mm. It is observed that the temperature histograms are spreading over a range of temperature of ~ 1000 K. It is obvious that there are two contributions to the value of the fluctuations of single-shot temperature measurements. One is due to the measurement error caused by the temperature CARS sensor, the other being related to the temporal local temperature fluctuations imposed by turbulence. To evaluate the value of both contributions, the first source of error was studied by performing CARS temperature measurements in an atmospheric pressure CH_4/air premixed flat flame exhibiting good temperature stability as well as good spatial uniformity. The results obtained on a sample of 500 single-shot temperature CARS measurements on H_2 at a temperature level of 2000 K allow to consider a temperature accuracy of 3%–4%. For H_2O , the accuracy of temperature is estimated equal to $\sim 6\%$ – 8% due to a lower sensitivity of the CARS profile with temperature. According to these values, the histograms presented in Fig. 6 are displayed with a class of temperature of 100 K representing the temperature error induced by the H_2 CARS temperature sensor. For $\text{O}/\text{F} = 1$, the temperature distributions are characterized by asymmetric distributions for radial positions ranging between $y = 0$ and 13 mm. This asymmetric distribution probably indicates that heat release from the reactive zone is still present in this region, avoiding a complete mixing of the hot gases coming from the annulus jet with the gas products of the core jet. For radial distance away from $y = 13$ mm, the temperature histogram is described by a Gaussian function indicating that the gaseous mixture is quite homogeneous. By increasing the mixture ratio at $\text{O}/\text{F} = 2$, the temperature histograms are naturally shifted towards the hot side with a mean temperature of ~ 2100 – 2300 K. The temperature histograms also broaden, probably due to a larger level of turbulence caused by a thickening of the reaction zone.

In Fig. 7, the mean temperature derived from the CARS measurements as well as the corresponding standard deviations are shown for H_2 and H_2O . Agreement of the H_2 and H_2O mean temperatures at each spatial position was at the maximum within ± 100 K, confirming the consistency of the data processing of

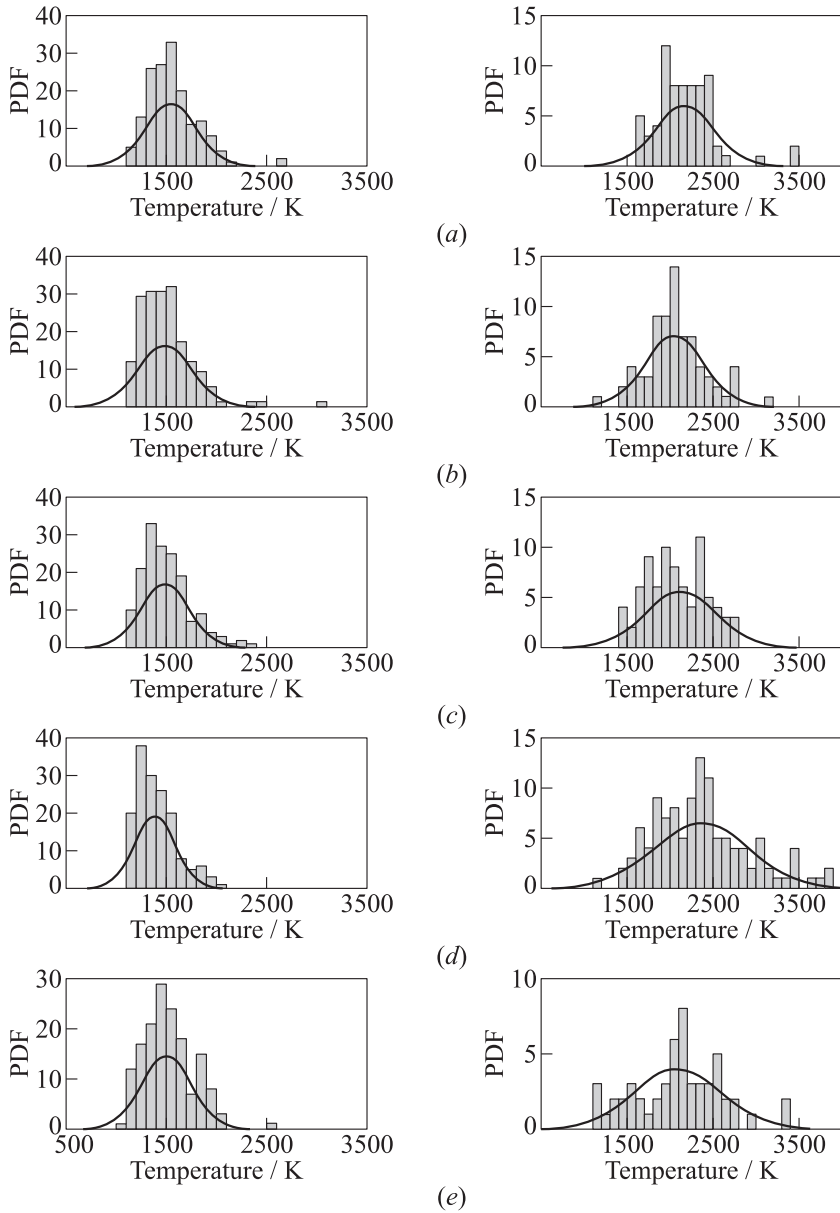


Figure 6 Temperature histograms deduced from H_2 CARS spectra at $y = 210$ mm downstream from the injector: left column — $O/F = 1$; right column — $O/F = 2$; (a) $x = 0$ mm; (b) 5; (c) 9; (d) 13; and (e) $x = 16.5$ mm

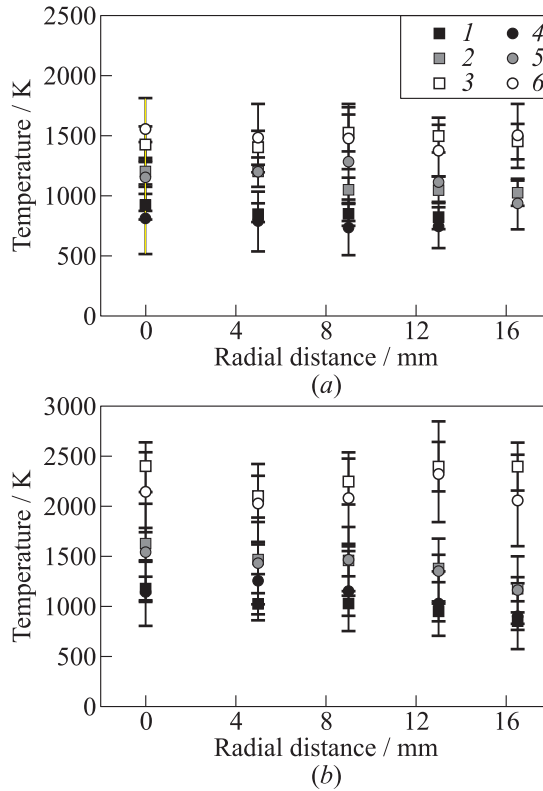


Figure 7 Temperature profiles deduced from H₂ (circles) and H₂O (squares) CARS spectra at various positions downstream from the injector. Mixture ratio O/F = 1 (a) and O/F = 2 (b): black signs — $x = 65$ mm; grey — 105; and empty signs — $x = 210$ mm

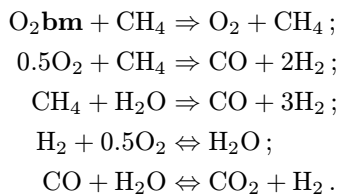
the CARS measurements for both molecules. The observed small discrepancies in measuring temperatures with both molecules can be partly explained by the existence of different sensitivities of the H₂ and H₂O CARS profiles to small change of temperature. Furthermore, the beam steering effects induced by the H₂ and H₂O geometrical arrangements of the laser beams can also be a source of distortion of the CARS measurements.

Whatever the mixture ratio, the evolution of the mean temperature increases downstream from the injector (see Fig. 7). The radial profiles of the mean temperatures are relatively flat that is not surprising at $x = 210$ mm where the flame closure is observed. Closer to the injection system, no peak temperature indicating the location of the flame front is noted. One reason which probably explains this observation comes from the mismatch between the CARS technique

allowing single-point measurements and the fineness of the flame front which requires, for its detection, a precise knowledge of its position. Many closely spaced positions must then be probed experimentally in order to precisely locate the flame front, which was unfortunately not the case in the current study.

4 COMPARISON BETWEEN EXPERIMENTAL AND NUMERICAL DATA

Numerical simulations of the reactive flowfield obtained for both mixture ratios $O/F = 1$ and 2 , were achieved using a $k-\omega$ shear stress transport (SST) turbulence model [21] with a turbulent Schmidt number of 0.7 . The combustion model is the TPaSR model including a 4-step global chemical-kinetic mechanism elaborated from Jones and Lindstedt [22]. The aim of the current model resides in the competition existing between the turbulent mixing and the chemical-kinetic reaction. To that end, O_2 is injected in the flowfield by two channels. O_2 bm (i. e., “b”efore “m”ixing) associated with a “mixed is burnt” model is first applied to “activate” O_2 bm (time scale = turbulent time scale) when mixed with CH_4 . Then, O_2 is burning following the 4-step chemical-kinetic mechanism. This procedure is only applied to O_2 bm since it is the only species injected into the central region of the reactive flowfield. The overall chemical-kinetic mechanism used in the current simulations is then the following:



The resulted distributions of temperature inside the combustion chamber for both mixture ratios are plotted in Fig. 8. The locations of the CARS measurements, as well as the optical window positions, are also indicated. The profiles of temperatures look like the ones calculated for a classical diffusion flame. In the near field of the injector, the region where chemical reactions occur is quite narrow. As seen in Fig. 8, the high-temperature region reaction zone occurs in an annular region until the flame tip is reached. The thickness of the high-temperature zone slowly increases indicating a weak diffusion of hot gases towards the external stream. Further downstream, i. e., in the flame closure region, there is a sufficient quantity of hot gases that buoyant forces become important. Buoyancy accelerates the flow and causes a narrowing of the flame, since conservation of mass requires streamlines to come closer together as the velocity increases. The narrowing of the flame increases the fuel concentration gradients,

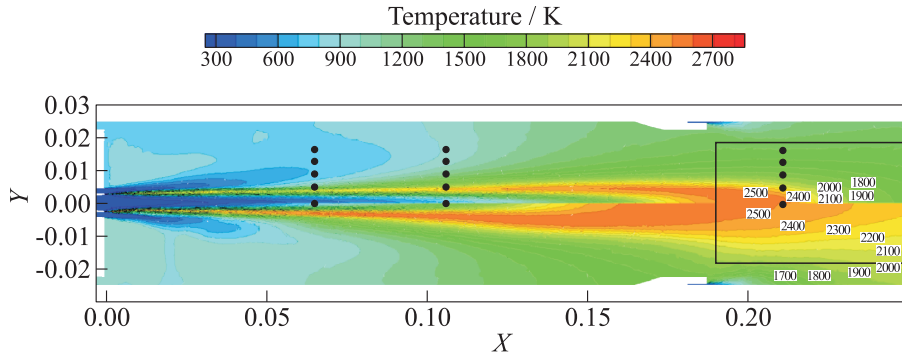


Figure 8 Computed temperature field for $O/F = 1$ (upper) and $O/F = 2$ (down).

thus enhancing diffusion. The temperature distribution then broadens, indicating the presence of an intense mixing between hot gases arising from the core jet and the ones coming from the external stream. A comparison between the temperature distributions simulated for both mixture ratios shows a faster increase of the reaction zone for $O/F = 2$ due to the enhancement of the combustion efficiency (higher level of temperature). As also observed experimentally, the flame length is longer in $O/F = 2$ than in $O/F = 1$.

Figure 9 displays the computed temperature profiles calculated for $x = 65$, 105, and 210 mm with the associated experimental CARS temperatures. The computed temperatures for both mixture ratios denote the existence of temperature distributions with very sharp gradients which are not observed experimentally. For instance, at $x = 210$ mm, the experimental mean temperature profile recorded for $O/F = 1$ is flat, typically around 1500 K, while the computation shows a sharp gradient of radial temperature from the axial flow axis to the outer wall. A maximum computed temperature around 2500 K is then observed on the flow axis with a fast decrease on the edges of the flame. Outside the chemical reaction zone, the computed temperature ranges between 1400 and 1600 K in good agreement with the experimental data. These behavioral differences, observed to some extent for all axial positions and for both mixture ratios, can be experimentally derived from the high intensity of turbulence and intermittent reactive processes observed during the experiments. These effects are not taken into account in the simulation since this computation is performed in a stationary case. The high level of turbulence favors the mixing of gases between the jet core and the outer stream leading to an average of temperature in time and in space and, consequently, reduces the presence of peak temperature which are undoubtedly overestimated in the numerical simulation.

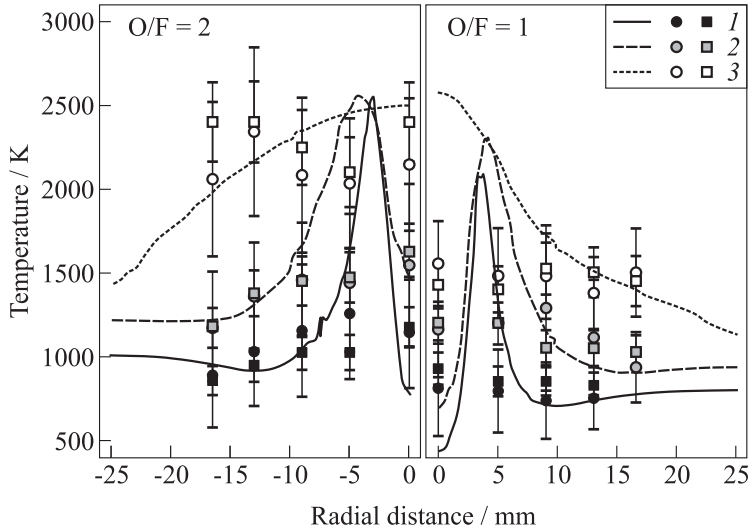


Figure 9 Comparison between the computed (curves) and the CARS (signs) temperature radial distributions for two mixture ratios: $O/F = 1$ (right) and $O/F = 2$ (left); circles — H_2 ; squares — H_2O ; 1 — $x = 65$ mm; 2 — 105; and 3 — $x = 210$ mm

The absence of computed OH concentration distributions avoids any direct interpretation of the experimental OH^* chemiluminescence spatial distributions. Nevertheless, complementary results on heat release simulations for both mixture ratios allow to give insights about the localization of intense chemical-kinetic reactions regions (Fig 10). The spatial opening of the heat release for $O/F = 2$ at distances larger than $x = 180$ mm is not due to the main chemical reactions occurring between O_2 and CH_4 since O_2 is already consumed at these locations,

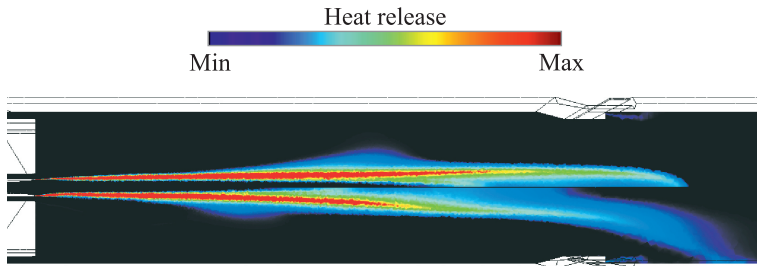
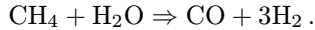


Figure 10 Heat release distribution for both mixture ratios: $O/F = 1$ (up) and $O/F = 2$ (down).

but is probably the consequence of chemical-kinetic reactions of species recombination such as the following chemical reaction:



The comparison between the location of heat release with the localization of OH^* in position 1 shows similar behaviors. The computed heat release is well located inside the mixing layer produced between the O_2 core jet with the outer methane jet as already observed on the experimental OH^* chemiluminescence distributions. On the contrary, the comparison between the zone of heat release with the OH^* production area in position 5 reveals discrepancies and, especially, for $\text{O}/\text{F} = 1$. As for temperature, this difference confirms the importance of the high level of turbulence encountered in these reactive flowfields which undoubtedly causes an intense gas mixing which leads to a thickening as well as a lengthening of the experimental flame.

5 CONCLUDING REMARKS

The combustion process in a high-pressure gaseous methane / gaseous oxygen rocket model combustor has been investigated by means of optical and laser spectroscopic measurements as well as numerical simulations. The application of CARS for temperature measurements in a gaseous CH_4/O_2 rocket model combustor at 1.0 MPa was successfully demonstrated. This work has been performed in the framework of the European project "In-Space Propulsion" (ISP). Single-shot temperature measurements were performed with a spatial resolution in beam direction of ~ 0.8 mm. Two CARS experimental setups were used to detect simultaneously H_2 and H_2O into the reactive flowfield. Temperature was deduced from the data processing of the H_2 and H_2O CARS spectra. The estimated accuracy of single-shot temperatures for H_2 is $\sim 3\%$ – 4% . For H_2O , the accuracy of temperature is estimated to about 6% – 8% . For each species, an ensemble of 150 instantaneous CARS measurements was recorded during each hot fire combustion test, for the different operating points of interest, defined by the pressure and the mixture ratio.

The temperature distributions display the degree of burnout which depends primarily on the mixing of H_2 and H_2O . Good agreement between the experimental temperature profiles deduced from the H_2 and the H_2O CARS spectra, in terms of mean and standard deviations, is observed. The high validation rates, defined as the ratio between the numbers of spectra successfully processed and the total number of laser shots, highlight the interest to use CARS in these severe conditions. Analyzing the complete set of data provides an insight of the flame structure which delivers a high level of turbulence as indicated by the standard

deviation of the instantaneous temperatures. The comparison between the experimental temperatures and those obtained from computational fluid dynamics simulations shows some discrepancies probably arising from the high level of turbulence which is not taken into account in the computations.

ACKNOWLEDGMENTS

This work was performed within the “ISP-1” project, coordinated by SNECMA, and supported by the European Union within the 7th Framework Program for Research & Technology (Grant agreement No. 218849).

REFERENCES

1. Candel, S., G. Herding, R. Snyder, P. Scoufflaire, C. Rolon, L. Vingert, M. Habiballah, F. Grisch, M. Péalat, P. Bouchardy, D. Stepowsky, A. Cessou, and P. Colin. 1998. Experimental investigation of shear coaxial cryogenic jet flames. *J. Propul. Power* 14:826–34.
2. Ivancic, B., W. Mayer, G. Krülle, and D. Brüggemann. 1999. Experimental and numerical investigation of time and length scales in LOx/GH₂-rocket combustors. *35th AIAA/ASME/SAE/ASEE Joint Propulsion Conference and Exhibit*. Los Angeles, CA, USA.
3. Arnold, R., D. Suslov, and O. J. Haidn. 2008. Experimental investigation of film cooling with tangential slot injection in LOx/CH₄ — subscale rocket combustion chamber. ISTS. Japan.
4. Slavinskaya, N. A., and O. J. Haidn. 2008. Reduced chemical model for high pressure methane combustion with PAH formation. AIAA Paper No. 2008-1012.
5. Yang, B., F. Cuoco, and M. Oswald. 2007. Atomization and flames in LOx/H₂- and LOx/CH₄ spray combustion. *J. Propul. Power* 23:763–71.
6. Pauly, C., J. Sender, and M. Oswald. 2007. Ignition of a gaseous methane/oxygen coaxial jet. *2nd European Conference for Aerospace Sciences (EUCASS)*. Brussels.
7. Haidn, O., G. Ordonneau, S. Soller, and M. Onofri. 2011. Oxygen–methane combustion studies in the In-Space Propulsion Programme. *4th European Conference for Aerospace Sciences (EUCASS)*. St.-Petersburg, Russia.
8. Grisch, F., P. Bouchardy, and W. Clauss. 2003. CARS thermometry in high pressure rocket combustors. *Aerosp. Sci. Technol.* 7:317–30.
9. Chaussard, F., X. Michaut, R. Saint-Loup, H. Berger, P. Bouchardy, and F. Grisch. 2004. Optical diagnostic of temperature in rocket engines by coherent Raman techniques. *C.R. Physique* 5:249–58.
10. Grisch, F., P. Bouchardy, L. Vingert, W. Clauss, M. Oswald, O. M. Stel'mack, and V. V. Smirnov. 2004. Coherent anti-Stokes Raman scattering measurements at high pressure in cryogenic LOx/GH₂ jet flames. In: *Liquid rocket thrust chambers*:

- Aspects of modeling, analysis and design.* Eds. V. Young, M. Habiballah, M. Popp, and J. Hulka. Progress in astronautics and aeronautics ser. Ch. 10. 200:369–404.
11. Jourdanneau, E., T. Gabard, F. Chaussard, R. Saint-Loup, H. Berger, E. Bertseva, and F. Grisch. 2007. CARS methane spectra: Experiments and simulations for temperature diagnostic purposes. *J. Molecular Spectroscopy* 246:167–79.
 12. Vingert, L., M. Habiballah, P. Vuillermoz, and S. Zurbach. 2000. Mascotte; a test facility for cryogenic combustion research at high pressure. *51st Astronautical Congress (International)*.
 13. Vingert, L., M. Habiballah, and P. Vuillermoz. 2002. Upgrading of the Mascotte cryogenic test bench to the LOx/methane combustion studies. *4th Conference (International) on Launcher Technology “Space Launcher Liquid Propulsion.”*
 14. Bourasseau, B. 1987. Programme de calcul des performances des systèmes propulsifs Coppelias. Onera RT 7/3589 EY.
 15. Dieke, G. H., and H. M. Crosswhite. 1962. The ultraviolet bands of OH: Fundamental data. *J. Quantitative Spectroscopy Radiative Transfer* 2:97–199.
 16. Regnier, P. R., and J. P. Taran. 1973. On the possibility of measuring gas concentrations by stimulated anti-Stokes scattering. *Appl. Phys. Lett.* 23:240–42.
 17. Druet, S., and J. P. Taran. 1981. CARS spectroscopy. *Prog. Quant. Electr.* 7:1–72.
 18. Greenhalgh, D. A. 1988. Quantitative CARS spectroscopy. In: *Advances in non-linear spectroscopy*. Eds. R. J. H. Clark and R. E. Hester. John Wileys & Sons. Vol. 15.
 19. Eckbreth, A. C. 1996. *Laser diagnostics for combustion temperature and species*. 2nd ed. Gordon and Breach Publ.
 20. Grisch, F. 2009. Coherent anti-Stokes Raman scattering (CARS) in combustion. In: *Laser diagnostics in combustion*. Ed. M. Lackner. Verlag ProcessEng Engineering GmbH.
 21. Menter, F. R. 1993. Zonal two equation $k-\omega$ turbulence models for aerodynamic flows. *24th AIAA Fluid Dynamic Conference Proceedings*. 1–21.
 22. Jones, W. P., and R. P. Lindstedt. 1988. Global reaction schemes for hydrocarbon combustion. *Combust. Flame* 73:233–49.